Electronic Supplementary Information

Ultrafast Joule Heating-Induced Formation of Amorphous CoFeNi Phosphate for Efficient and Stable Oxygen Evolution Reaction

Junhao Ma,[1,‡] Chonghan Xia,[1,‡] Teddy Salim,[1] Yee Yan Tay,[1] Lydia H. Wong,[1] and Kwan W. Tan[1,*]

Affiliations:

[1]School of Materials Science and Engineering, Nanyang Technological University, Singapore 639798, Singapore.

[‡]These authors contribute equally to the work.

*Correspondence: kwtan@ntu.edu.sg

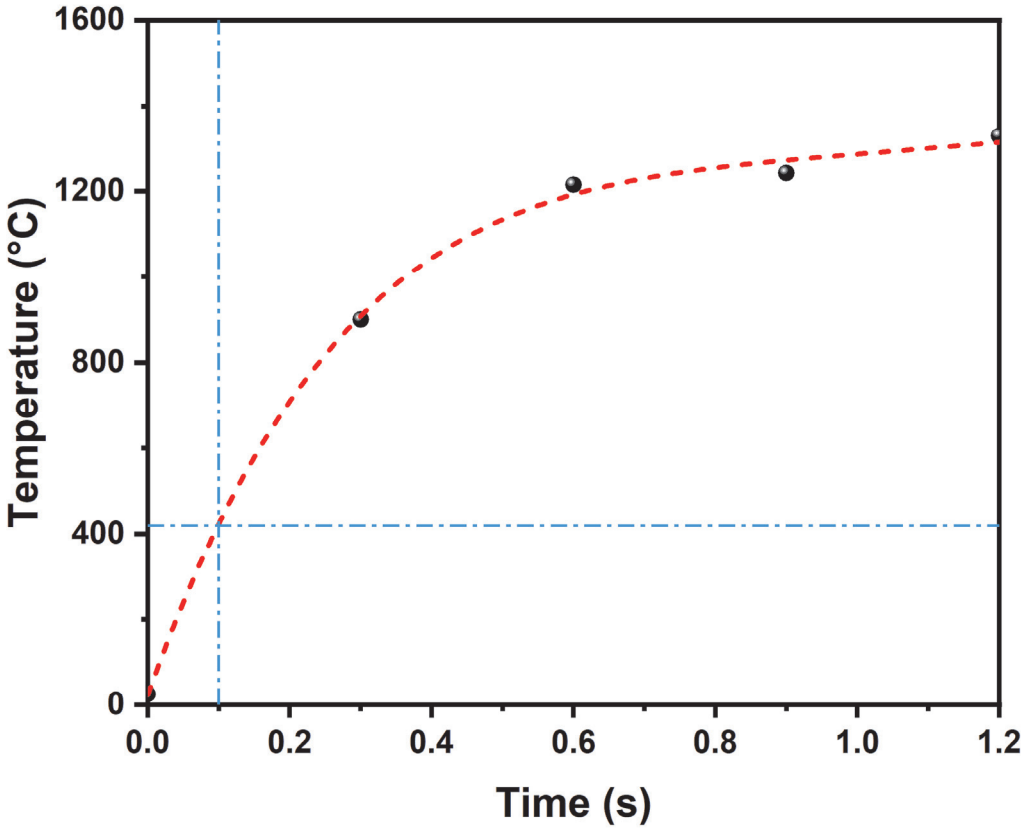

Figure S1. Empirical plot of infrared temperature versus heating time during Joule heating set at 22 V and 20 A. The red-colored dashed line represents the results obtained from polynomial regression analysis using the data points. The horizonal and vertical blue dashed-dotted lines indicate the estimated temperature for a 100 ms heating time is ~420 °C.

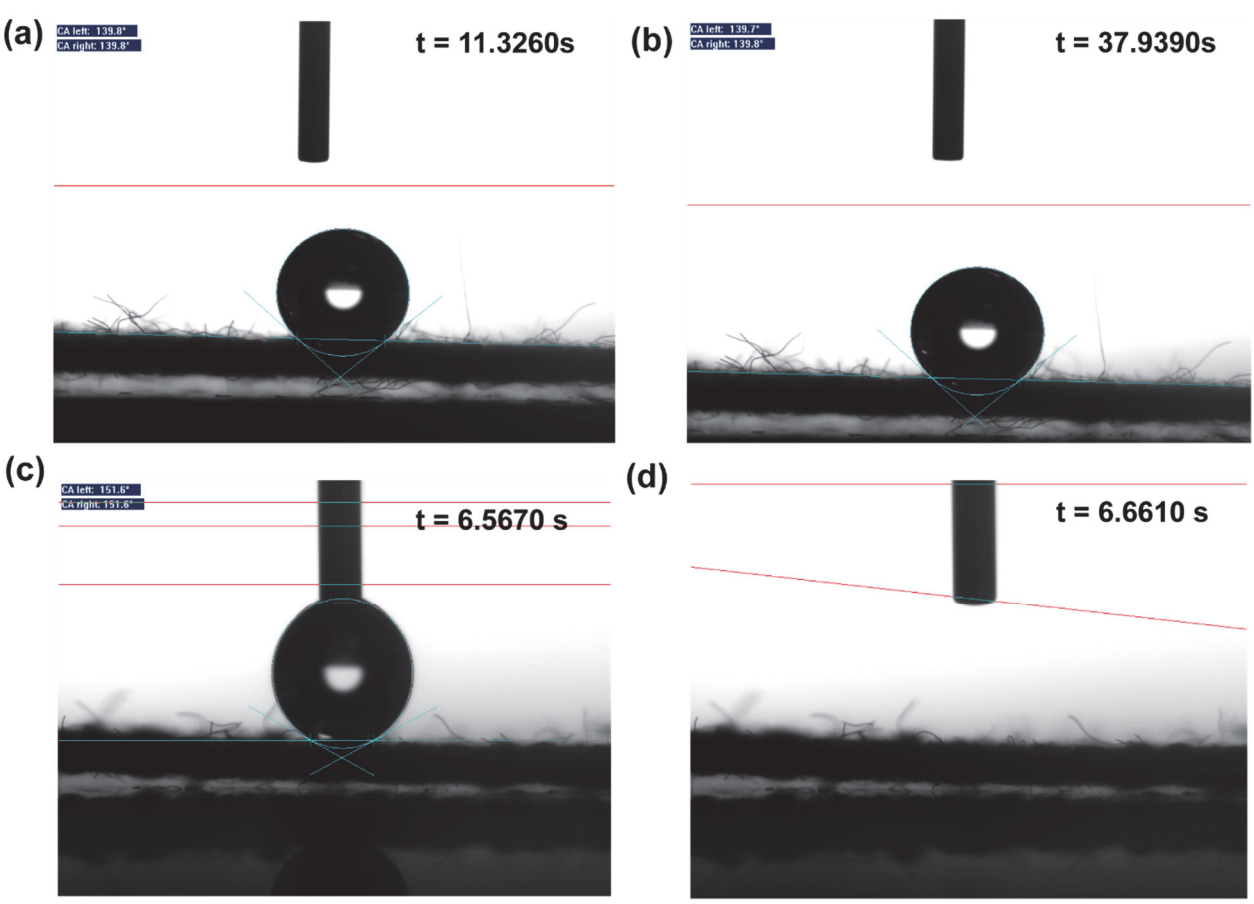

Figure S2. Water contact angle measurements were conducted on (a, b) original carbon cloth and (c, d) heat-treated and KOH-activated carbon cloth (ACC). The water droplet contact angle on the original carbon cloth remained ~139.8° even after a waiting time of 26 s (a and b), indicating its hydrophobic nature. In contrast, water droplets wet the surface of ACC in less than 0.2 s (c and d), confirming that ACC is superhydrophilic.

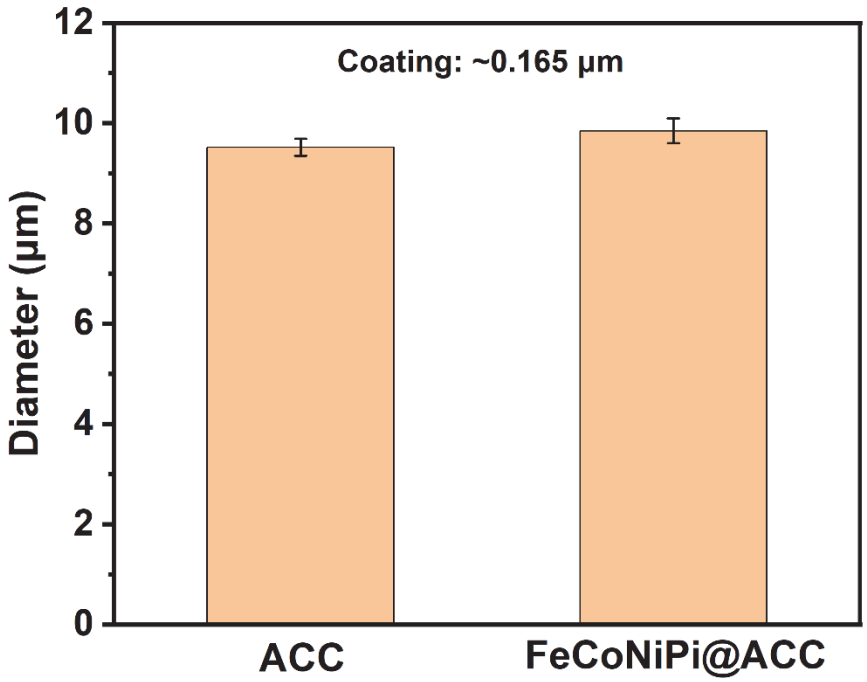

Figure S3. The bar charts display diameter measurements of individual uncoated ACC fibers and CoFeNiPi@ACC fibers after Joule heating. The thickness of the CoFeNiPi@ACC coating is around 165 nm.

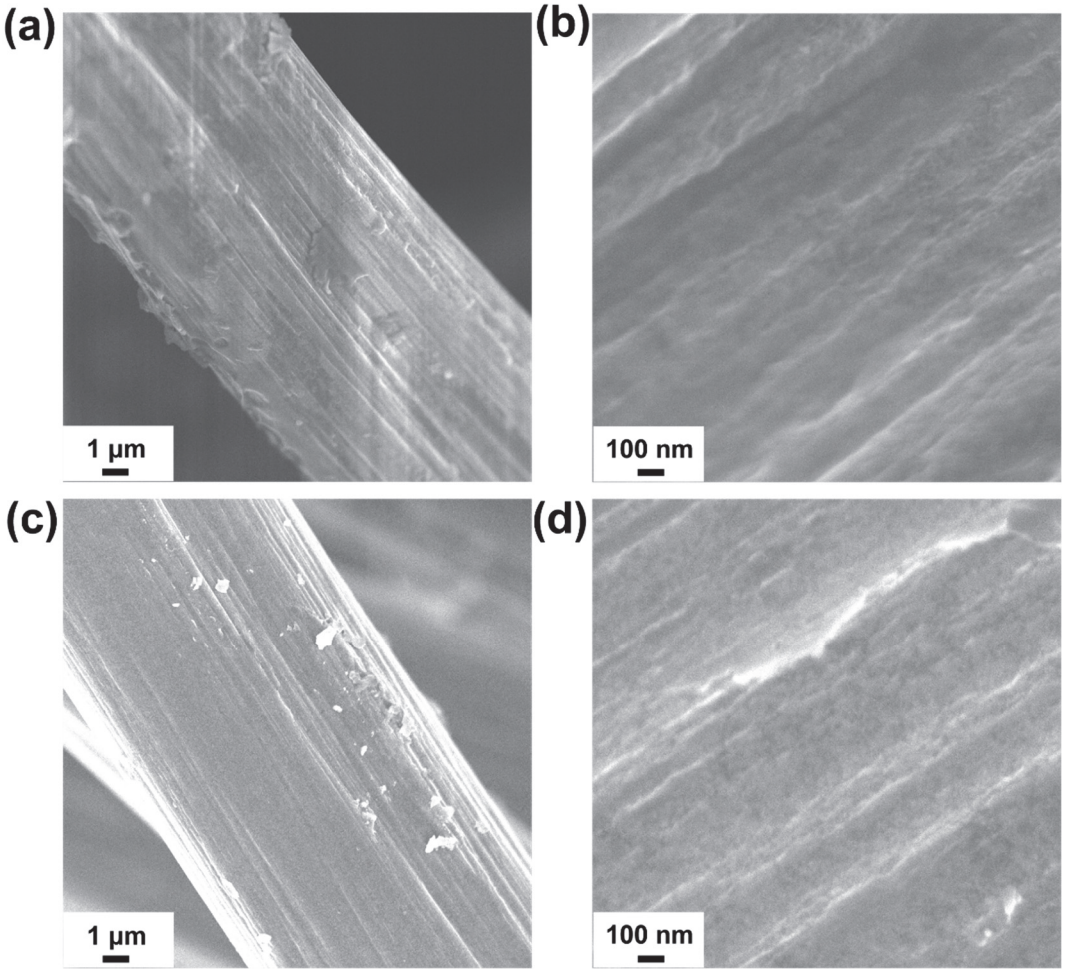

Figure S4. SEM micrographs show the relatively smooth surfaces of (a, b) CoPi@ACC and (c, d) CoFePi@ACC after Joule heating for 100 ms at ~420 °C.

Table S1. Atomic percentages of CoFeNiPi@ACC as determined by HAADF-STEM EDS.

Element	CoFeNiPi@ACC	CoFeNiPi@ACC-24h
Ni	1.84	2.16
Co	1.73	1.60
Fe	2.36	2.12
P	18.29	4.12
O	75.78	89.99

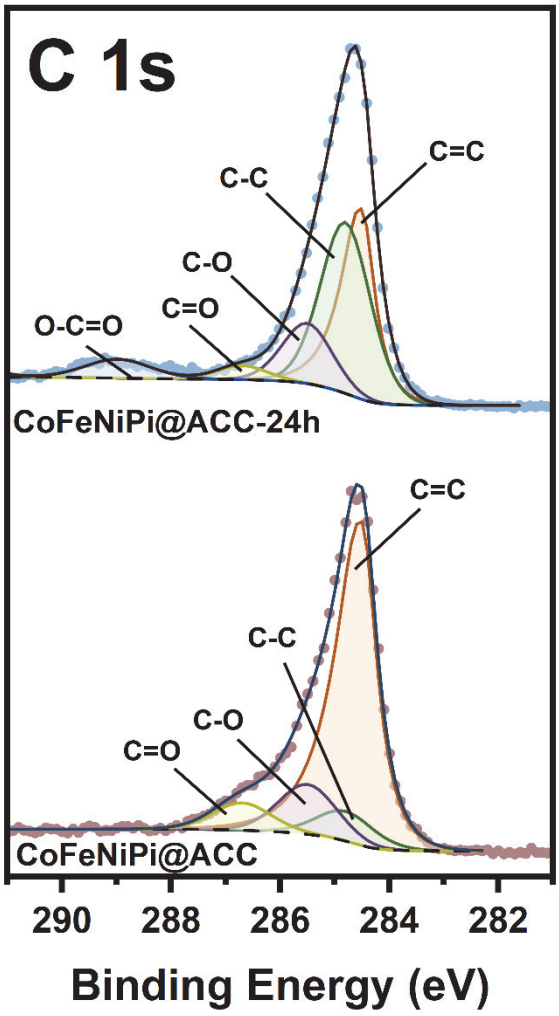

Figure S5. XPS analysis of CoFeNiPi@ACC and CoFeNiPi@ACC-24h samples showing the C 1s spectrum .

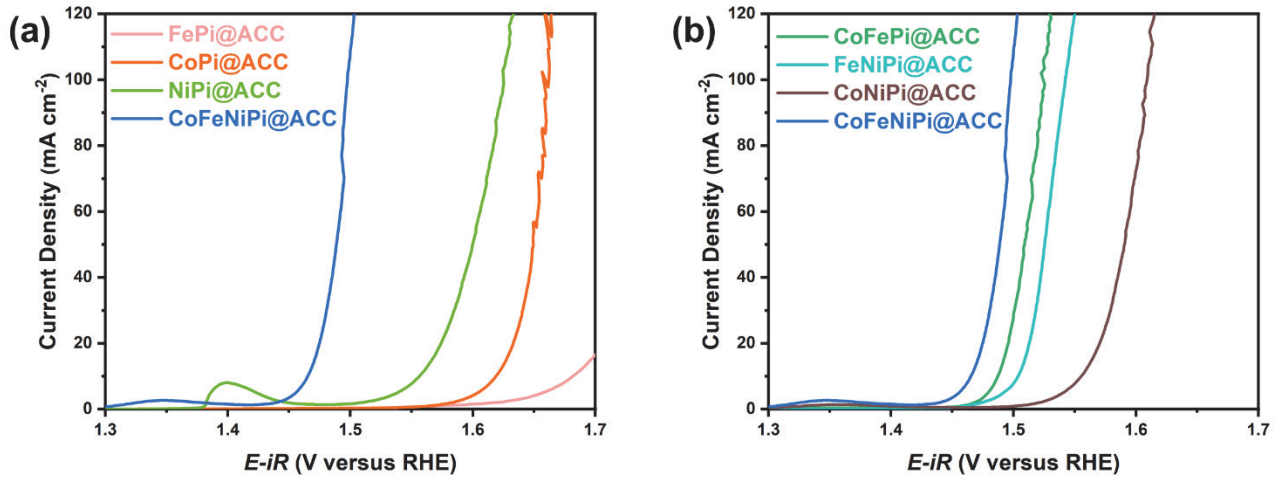

Figure S6. Polarization curves of (a) amorphous unary metal phosphates and (b) amorphous binary metal phosphates, compared to CoFeNiPi@ACC.

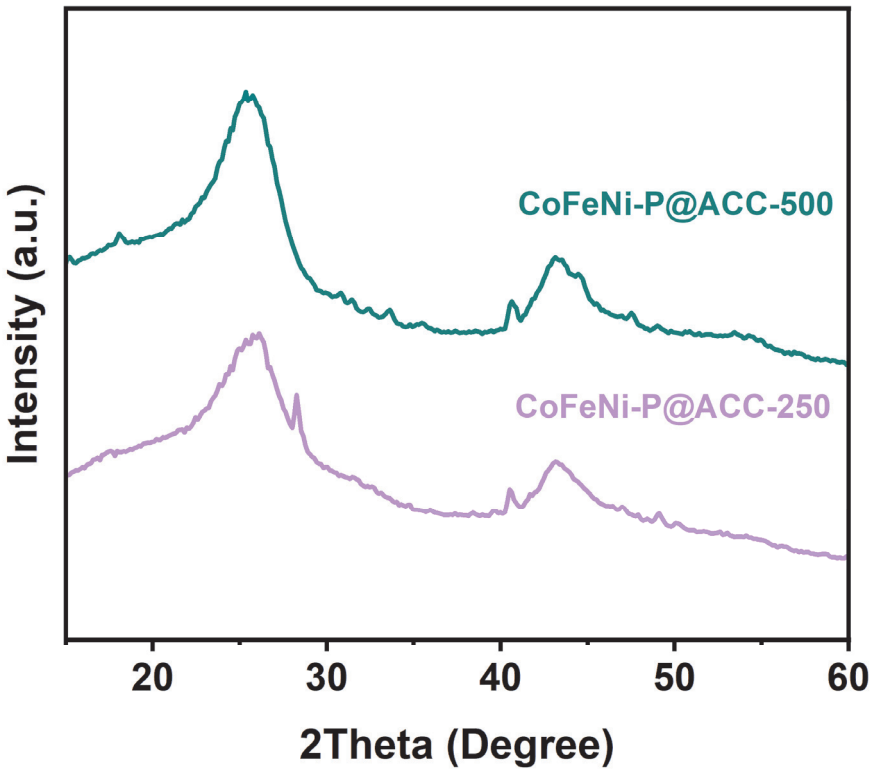

Figure S7. WAXS patterns of CoFeNi-based phosphorous-containing samples that were Joule heated for 250 ms (violet curve) and 500 ms (green curve) show the appearance of new reflections, indicating that both samples are crystalline.

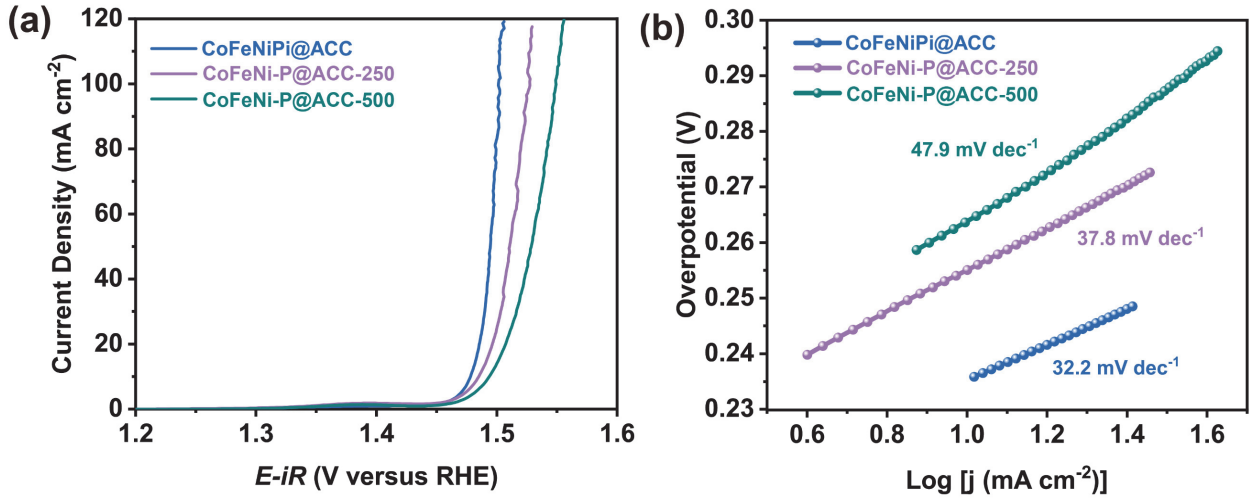

Figure S8. (a) Polarization curves and (b) Tafel slopes of crystalline CoFeNi-P@ACC-250 and crystalline CoFeNi-P@ACC-500, compared to amorphous CoFeNiPi@ACC. To drive a 100 mA cm^{-2} current density, the overpotential value of amorphous CoFeNiPi@ACC is the lowest (267 mV), compared to crystalline CoFeNi-P@ACC-250 (298 mV) and crystalline CoFeNi-P@ACC-500 (319 mV). Additionally, the amorphous CoFeNiPi@ACC has the lowest Tafel slope (32.2 mV dec^{-1}), compared to the crystalline CoFeNi-P@ACC-250 (37.8 mV dec^{-1}) and crystalline CoFeNi-P@ACC-500 (47.9 mV dec^{-1}).

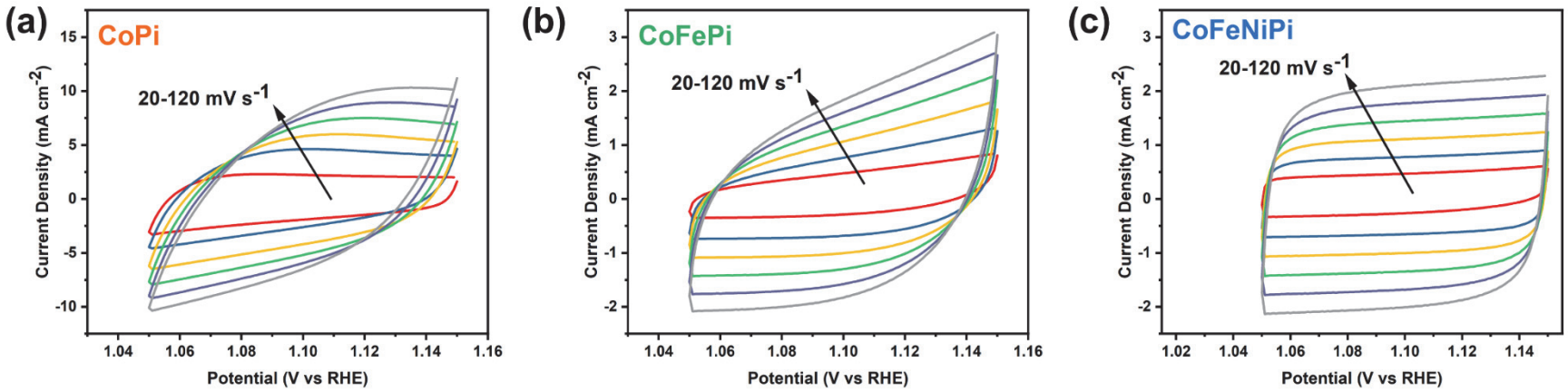

Figure S9. Cyclic voltammetry plots of the amorphous metal phosphate catalysts measured between 1.05 to 1.15 V at various scan rates from 20 to 120 mV s^{-1}: (a) CoPi@ACC, (b) CoFePi@ACC, and (c) CoFeNiPi@ACC.

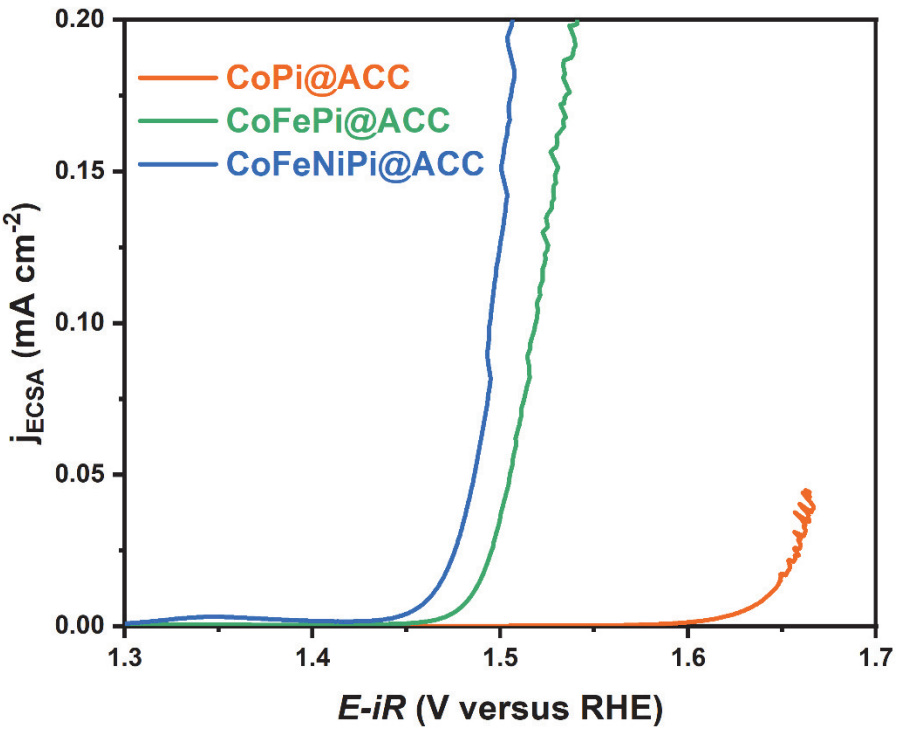

Figure S10. Polarization curves of amorphous metal phosphates as a function of electrochemical surface area (ECSA).

Table S2. Summary of the OER performance of recent phosphate-based electrocatalysts in alkaline media.

Electrocatalyst	η_{10}/mV	Tafel slope/mV dec^{-1}	ECSA/cm^2	Ref.
FeCoNiPi@ACC	235	32.2	430	This work
NiCoFeMnMoPi	270	74	-	1
$Ni_{1.5}Sn$@triMPO_4	240	45.2	-	2
CoNiPi@V-Co_4N	270	54.7	9655	3
$Co_{1.6}Ni_{0.4}P_4O_{12}$-C	230	51.1	432.5	4
$Co_3(OH)_2(HPO_4)_2$/NF	240	69	107.5	5
TiO_2|$Co_2P_4O_{12}$	330	44	-	6
V-Fe_2/$FePO_4$	270	45.1	454	7

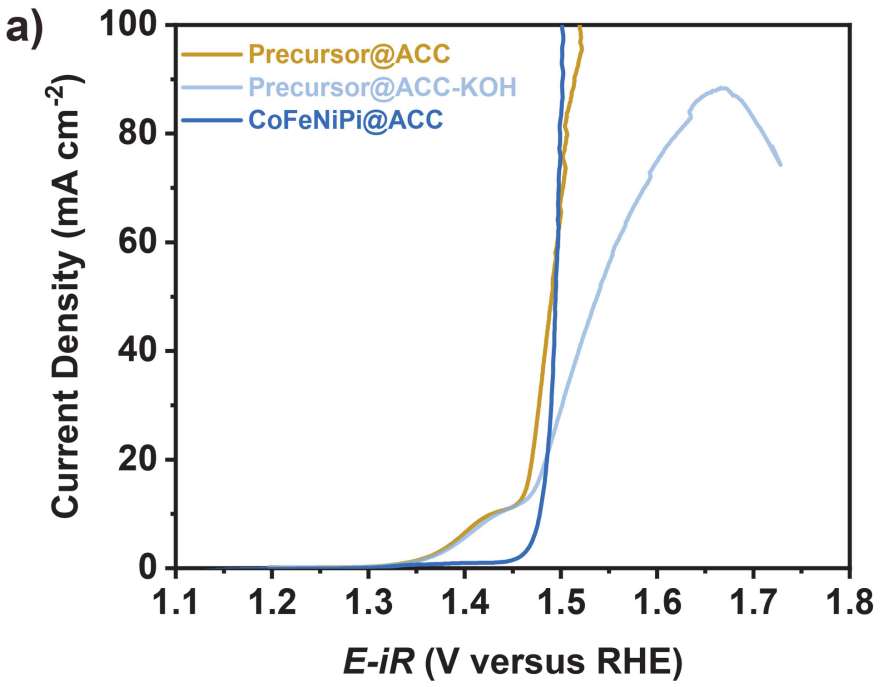

b)

ICP-OES result			
	Fe/mg L^{-1}	Co/mg L^{-1}	Ni/mg L^{-1}
KOH (CoFeNiPi@ACC-KOH)	–	–	–
KOH (Precursor@ACC-KOH)	0.369	–	–

Figure S11. (a) Polarization curves of Joule heating-induced amorphous CoFeNiPi@ACC compared with those of metal salt/phytic acid precursor coated on the ACC, activated and after immersion in 1 M KOH for 3 h. (b) Summary of ICP-OES results showing the leached metal content after amorphous CoFeNiPi@ACC and precursor@ACC were immersed in 1 M KOH for 3 h.

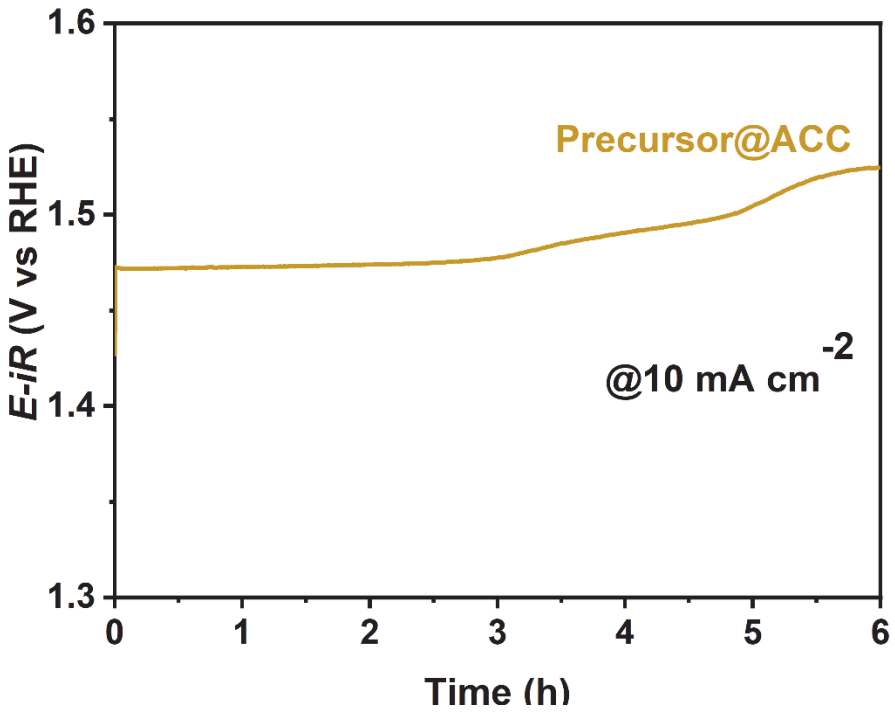

Figure S12. Chronopotentiometry curve for metal salt/phytic acid precursor@ACC over 6 h at a constant current density of 10 mA cm^{-2}.

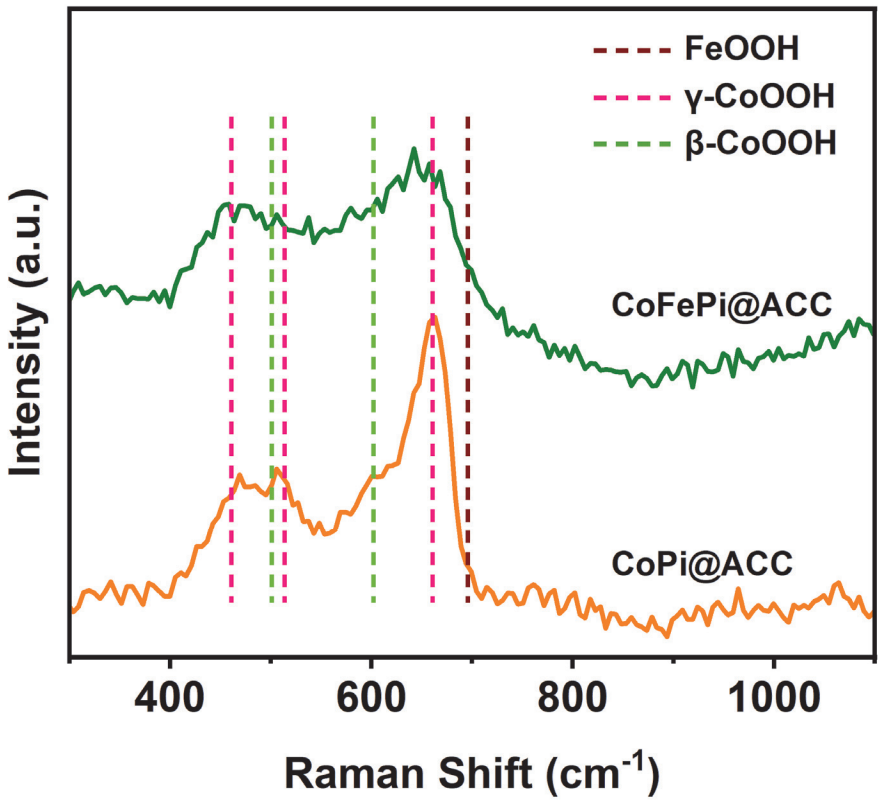

Figure S13. Raman spectra of CoPi@ACC and CoFePi@ACC in the activated state.

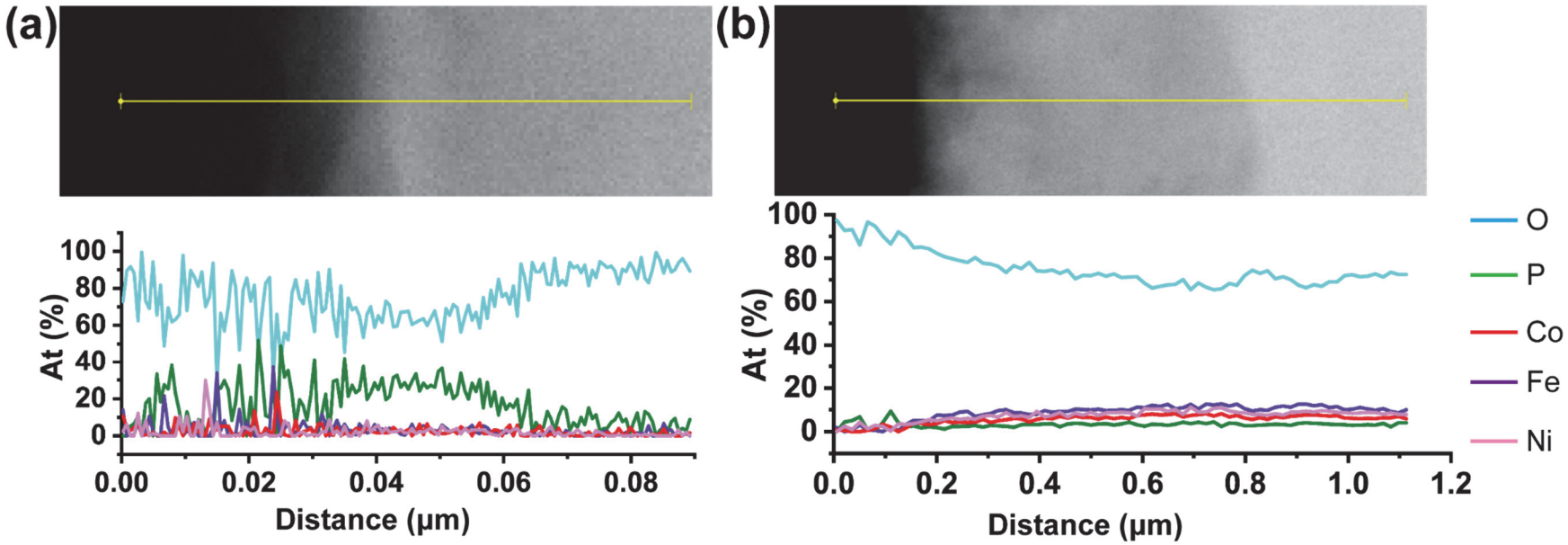

Figure S14. EDS line scan analysis of the CoFeNiPi@ACC catalysts in the (a) as-made state after Joule heating and (b) after chronopotentiometry at a constant current density of 10 mA/cm² for 100 h.

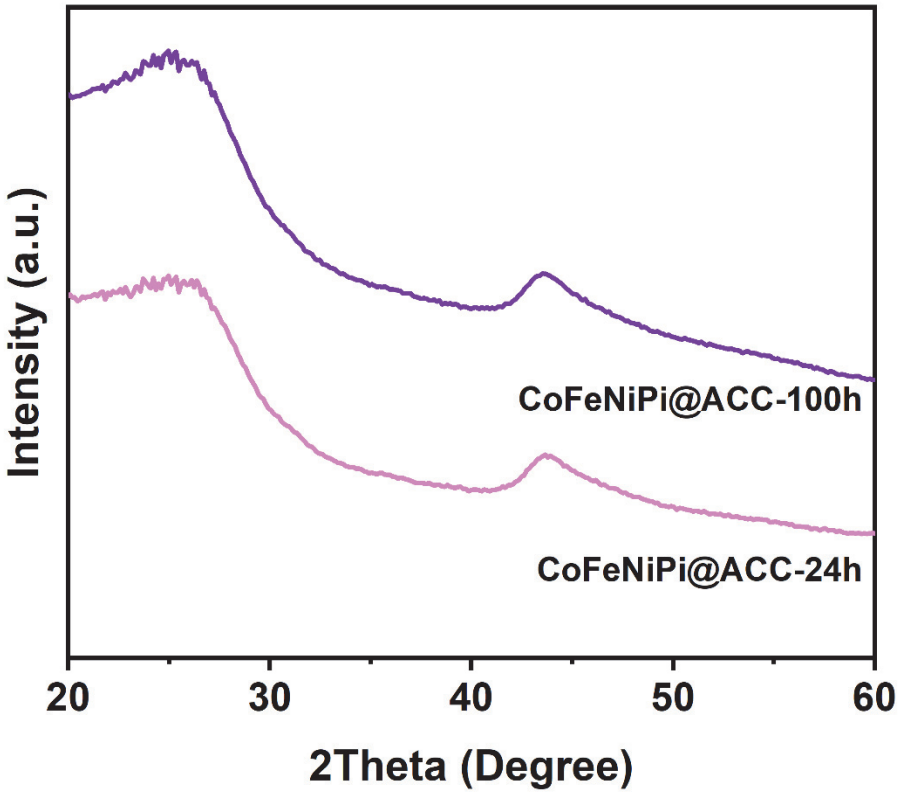

Figure S15. WAXS spectra of CoFeNiPi@ACC catalysts after chronopotentiometry at a constant current density of 10 mA cm^{-2} over 24 and 100 h.

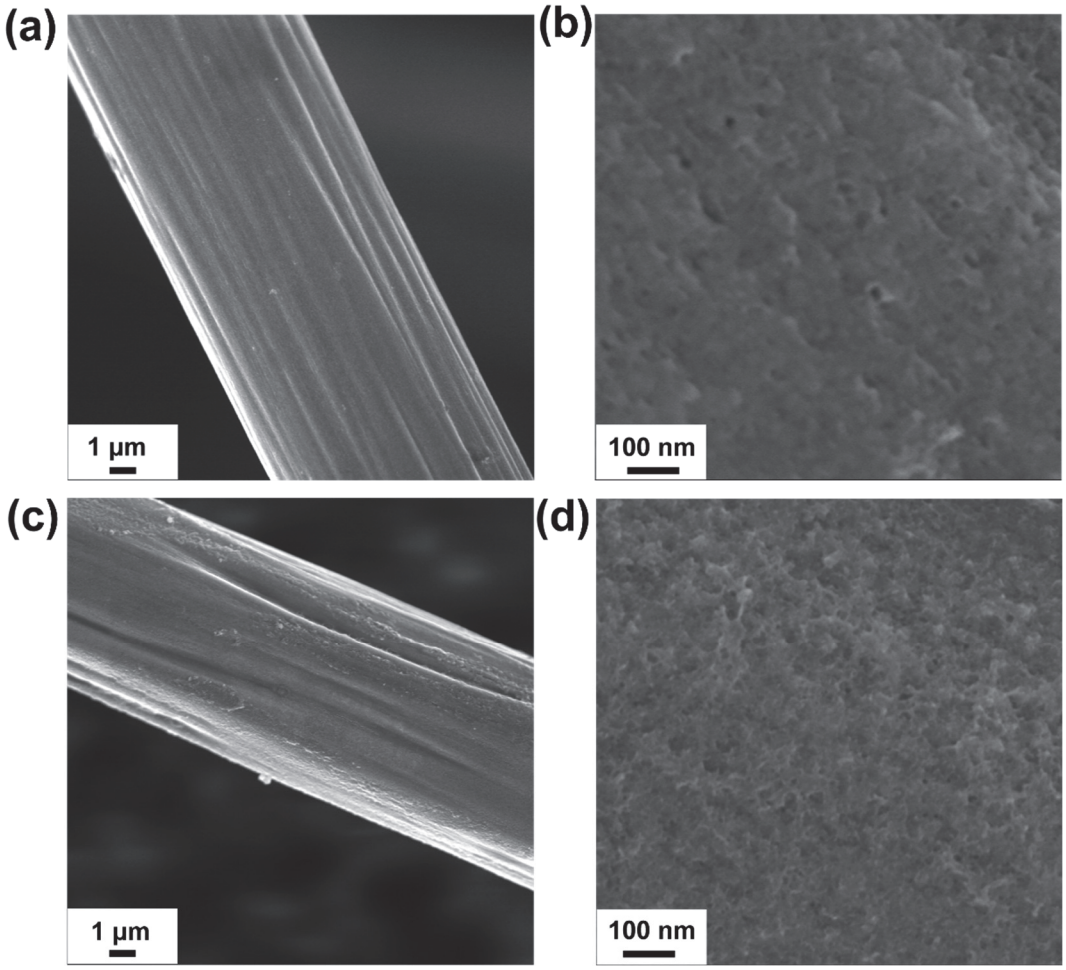

Figure S16. SEM images of CoFePi@ACC catalysts after chronopotentiometry at a constant current density of 10 mA cm^{-2} for (a,b) 24 h and (c, d) 100 h.

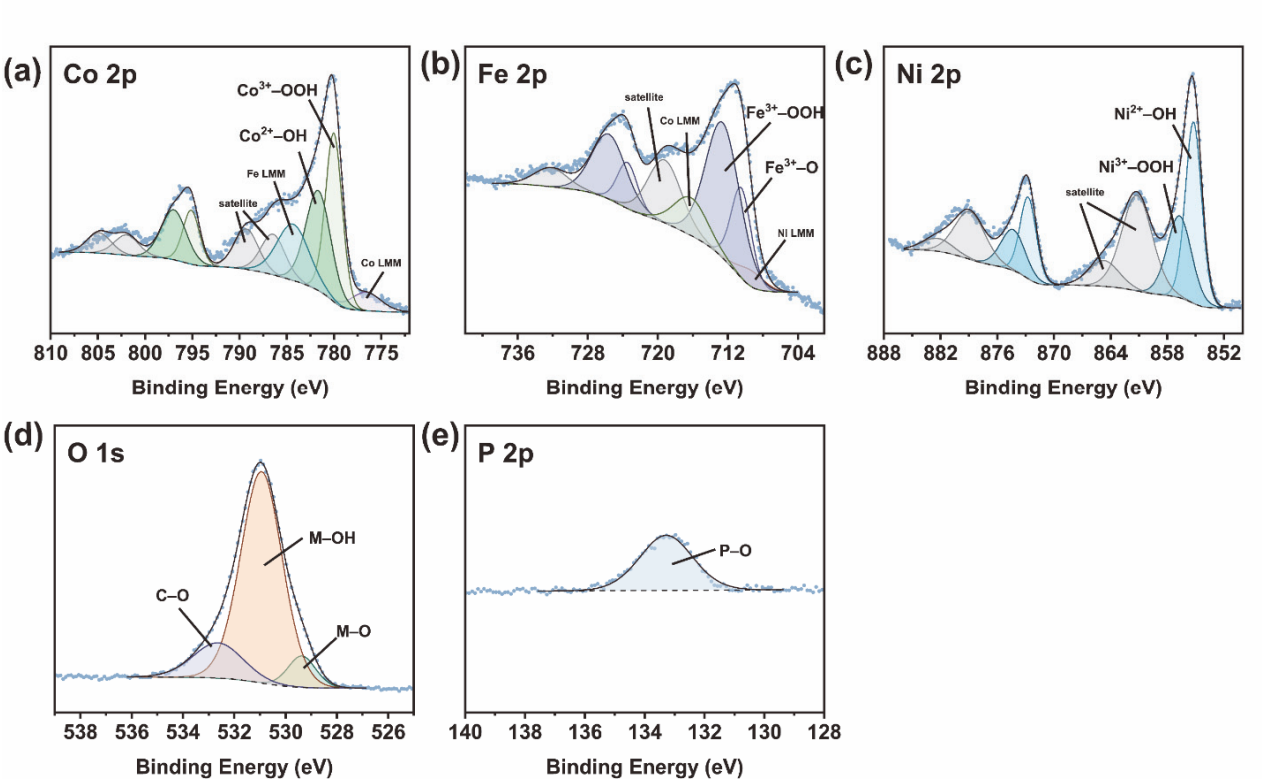

Figure S17. XPS analysis of CoFeNiPi@ACC-100h sample showing the spectra of (a) Co 2p, (b) Fe 2p, (c) Ni 2p, (d) O 1s, and (e) P 2p.

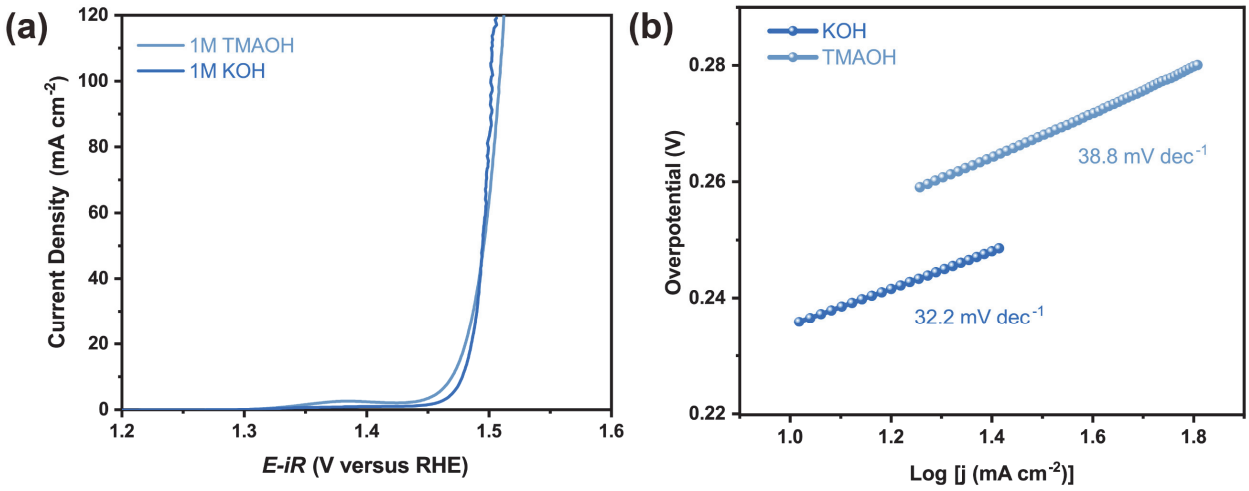

Figure S18. (a) Polarization curves and (b) Tafel slopes of ternary metal phosphate CoFeNiPi@ACC in TMAOH compared to KOH.

Reference

(1) Qiao, H.; Wang, X.; Dong, Q.; Zheng, H.; Chen, G.; Hong, M.; Yang, C.-P.; Wu, M.; He, K.; Hu, L. *Nano Energy* **2021**, *86*, 106029.

(2) Li, S.; Li, Z.; Ma, R.; Gao, C.; Liu, L.; Hu, L.; Zhu, J.; Sun, T.; Tang, Y.; Liu, D.; Wang, J. *Angew. Chem., Int. Ed.* **2021**, *60* (7), 3773–3780.

(3) Singh, T. I.; Maibam, A.; Cha, D. C.; Yoo, S.; Babarao, R.; Lee, S. U.; Lee, S. *Adv. Sci.* **2022**, *9* (23), 2201311.

(4) Li, Y.; Wang, Z.; Hu, J.; Li, S.; Du, Y.; Han, X.; Xu, P. *Adv. Funct. Mater.* **2020**, *30* (25), 1910498.

(5) Menezes, P. W.; Panda, C.; Walter, C.; Schwarze, M.; Driess, M. *Adv. Funct. Mater.* **2019**, *29* (32), 1808632.

(6) Lv, C.; Xu, S.; Yang, Q.; Huang, Z.; Zhang, C. *J. Mater. Chem. A* **2019**, *7* (20), 12457–12467.

(7) Ngo, Q. P.; Nguyen, T. T.; Singh, M.; Balaji, R.; Kim, N. H.; Lee, J. H. *Appl. Catal., B* **2023**, *331*, 122674.